Urban Expansion in the Earth System

A Reduced-Form Eco-Climate Laboratory for Infrastructure–Carbon–Climate Feedbacks

Flyxion

March 10, 2026

Abstract

Climate dynamics, carbon cycle feedbacks, and urban land transformation are typically studied within separate scientific traditions: climate models focus on radiative forcing and ocean heat uptake; carbon cycle research investigates biospheric productivity and oceanic exchange; and urban science examines infrastructure morphology and demographic drivers of land conversion. These systems interact physically, however, through multiple coupled pathways including radiative forcing, surface-albedo modification, suppression of evapotranspiration, acceleration of soil respiration, and the replacement of biologically productive landscapes by impervious built surfaces.

This paper introduces a reduced-form modeling framework that integrates climate dynamics, atmospheric chemistry, terrestrial carbon processes, and urban infrastructure expansion within a unified simulation environment. The framework couples a two-layer energy-balance climate model with a simplified carbon cycle and stylized infrastructure growth trajectories. Nitrous oxide is incorporated as an additional long-lived greenhouse gas whose atmospheric lifetime is sensitive to stratospheric loss processes. Through a coupled system of ordinary differential equations, the model embeds infrastructure expansion as a simultaneous modifier of planetary radiative balance and terrestrial carbon uptake, creating a feedback loop that conventional sectoral analyses cannot easily represent.

Numerical experiments across four illustrative scenarios—a moderate baseline, rapid infrastructure expansion, ecological restoration, and elevated nitrous oxide emissions—demonstrate how different development trajectories produce divergent long-term temperature and atmospheric composition outcomes. Phase portrait analysis and equilibrium climate sensitivity curves further illuminate the parametric structure of the system. The framework provides a conceptual laboratory particularly suited for exploring structural mechanisms that become difficult to isolate within large Earth system models, while remaining transparent enough to permit analytical interrogation of its governing equations.

Contents

1 Introduction **3**

2 Two-Layer Energy Balance Climate Model **4**

3 Carbon Dioxide Forcing and Carbon Cycle **5**
3.1 Radiative Forcing from CO_2 5
3.2 Atmospheric CO_2 Dynamics 5
3.3 Terrestrial Carbon Uptake 6
3.4 Oceanic Carbon Uptake 6

4 Nitrous Oxide Dynamics **7**
4.1 Atmospheric Mass Balance 7
4.2 Radiative Forcing from N_2O 7

5 Urban Infrastructure and Land Transformation **7**
5.1 Infrastructure Growth Trajectories 7
5.2 Thermal Forcing from Built Surfaces 8

6 Coupled System and Parameter Calibration **8**
6.1 Governing Equations 8
6.2 Parameter Values 9

7 Scenario Experiments and Results **9**
7.1 Scenario Definitions 9
7.2 Temperature and Forcing Trajectories 11
7.3 Carbon Cycle Feedbacks and Land Transformation 11
7.4 Sensitivity Analysis: Climate Feedback and Phase Structure 11

8 Discussion **13**
8.1 Infrastructure as a Secondary Climate Forcing 13
8.2 Limitations and Model Assumptions 15
8.3 Directions for Extension 15

9 Conclusion **16**

1 Introduction

Global climate dynamics are commonly studied using either comprehensive Earth system models (ESMs) or reduced-form energy-balance models that capture the dominant physical processes governing planetary temperature response. Urban expansion and infrastructure growth are, in parallel, investigated within a separate literature focused on land-use change, spatial development patterns, and the economic and demographic forces shaping cities (Batty, 2013; Angel et al., 2011; Seto et al., 2012).

This disciplinary separation creates a structural gap in our understanding of the Earth system. Human infrastructure does not merely consume energy and produce greenhouse gas emissions. It also modifies planetary energy balances through changes in surface albedo, evapotranspiration, and heat storage, while simultaneously transforming biologically productive landscapes that regulate atmospheric carbon. Urbanization therefore interacts with the climate system through at least three distinct physical pathways.

Direct thermal forcing. Built surfaces—concrete, asphalt, rooftops, and road networks—have lower albedo and higher heat capacity than the vegetated or bare soils they replace. These properties generate the urban heat island (UHI) effect that has been documented across biomes and climate zones (Oke, 1982; Zhao et al., 2014; Imhoff et al., 2010). At global scales, the aggregate thermal perturbation associated with impervious surface expansion constitutes a small but non-negligible positive radiative forcing.

Indirect carbon cycle forcing. Urban expansion replaces terrestrial ecosystems that participate in carbon uptake. The conversion of forests, grasslands, and wetlands to built land reduces the area available for photosynthesis and above-ground carbon storage, while simultaneously exposing soil carbon to enhanced oxidation and temperature stress (Davidson and Janssens, 2006). As global urban land area is projected to expand substantially over the coming decades (Seto et al., 2012), the associated loss of productive land may weaken terrestrial carbon sinks and amplify atmospheric carbon accumulation.

Road network fragmentation. Linear infrastructure such as roads and railways fragments ecosystems and modifies hydrological pathways, altering soil moisture regimes and thereby influencing both soil respiration rates and the partitioning of net ecosystem productivity. Although these effects are spatially heterogeneous, their cumulative contribution to carbon cycle dynamics may be significant at continental scales.

Despite these connections, most climate modeling frameworks treat urban land transformation as an external boundary condition rather than a dynamically coupled component of the Earth system. Urban science, conversely, often focuses on socioeconomic and morphological dynamics without explicitly representing planetary energy and carbon feedbacks.

This paper introduces a reduced-form simulation framework designed to close this gap at a conceptual level. The goal is not predictive accuracy—the framework lacks the spatial resolution and process complexity required for quantitative projection—but structural transparency. By coupling a two-layer energy-balance climate model with simplified carbon cycle dynamics, nitrous oxide chemistry, and stylized infrastructure growth trajectories, the

model creates a laboratory in which individual feedback mechanisms can be examined and compared in isolation or combination.

The energy-balance climate model draws on classical analyses of climate sensitivity and feedback mechanisms (Hansen et al., 1984) and on later calibrations of two-layer models against CMIP5 general circulation model output (Geoffroy et al., 2013). Radiative forcing from carbon dioxide follows the logarithmic parameterization of Myhre et al. (1998). Terrestrial carbon cycle dynamics draw on empirical work on soil carbon and temperature-dependent respiration (Parton et al., 1987; Lloyd and Taylor, 1994; Davidson and Janssens, 2006). Long-term projections of nitrous oxide incorporate recent understanding of stratospheric loss uncertainty (Prather and Wilson, 2026).

The remainder of the paper is organized as follows. Sections 2 through 4 introduce the governing equations for each model component. Section 6 describes how the components are coupled into a unified system. Section 6.2 documents parameter choices. Section 7 presents scenario experiments and numerical results. Sections 8 and 9 discuss implications and directions for future work.

2 Two-Layer Energy Balance Climate Model

The climate component of the framework is represented using the two-layer energy-balance model (EBM) introduced and calibrated by Geoffroy et al. (2013). This model partitions the ocean–atmosphere system into a rapidly responding mixed layer and a slowly equilibrating deep ocean, capturing the transient behavior of coupled general circulation models with a minimal set of parameters.

Let $T_m(t)$ denote the global mean temperature anomaly of the mixed surface layer and atmosphere relative to a preindustrial reference state, and let $T_d(t)$ denote the corresponding temperature anomaly of the deep ocean. The governing equations are

$$C_m \frac{dT_m}{dt} = F_{\text{tot}} - \lambda\, T_m - \kappa\,(T_m - T_d), \tag{1}$$

$$C_d \frac{dT_d}{dt} = \kappa\,(T_m - T_d), \tag{2}$$

where

- C_m [$\mathrm{W\,yr\,m^{-2}\,K^{-1}}$] is the effective heat capacity of the mixed layer and troposphere,
- C_d [$\mathrm{W\,yr\,m^{-2}\,K^{-1}}$] is the effective heat capacity of the deep ocean,
- λ [$\mathrm{W\,m^{-2}\,K^{-1}}$] is the net climate feedback parameter (positive values indicate a stabilizing feedback),
- κ [$\mathrm{W\,m^{-2}\,K^{-1}}$] is the inter-layer heat exchange coefficient, and
- $F_{\text{tot}}(t)$ [$\mathrm{W\,m^{-2}}$] is the total radiative forcing, decomposed in Section 6.

Equilibrium and transient response. Setting both time derivatives to zero and noting that equilibrium requires $T_m = T_d$ yields the equilibrium climate sensitivity (ECS),

$$\mathrm{ECS} = \frac{F_{\mathrm{tot}}^{\infty}}{\lambda}, \tag{3}$$

where $F_{\mathrm{tot}}^{\infty}$ is the sustained long-term forcing. For a CO_2 doubling, $F_{\mathrm{tot}}^{\infty} = F_{2\times}$ and $\mathrm{ECS} = F_{2\times}/\lambda$. The transient climate response (TCR)—the warming at the time of CO_2 doubling in a 1% per year increase experiment—is lower than the ECS because deep-ocean heat uptake suppresses the surface response on decadal timescales (Gregory et al., 2004).

Proposition 1 (Analytical steady state)**.** *In the long-time limit with constant forcing F_0, the system (1)–(2) has the unique stable equilibrium $T_m^* = T_d^* = F_0/\lambda$.*

Proof. At steady state, $dT_m/dt = 0$ and $dT_d/dt = 0$. Equation (2) immediately gives $T_m^* = T_d^*$. Substituting into (1) gives $F_0 = \lambda T_m^*$, hence $T_m^* = F_0/\lambda$. Stability follows from the negative eigenvalues of the linearized system, which are real and negative for $\lambda, \kappa > 0$. □

Remark 1. *The parameter κ controls the rate at which the surface equilibrates to its steady state but does not affect the long-run ECS. Larger κ speeds convergence of T_d toward T_m, reducing the realized warming on centennial timescales.*

3 Carbon Dioxide Forcing and Carbon Cycle

3.1 Radiative Forcing from CO_2

The radiative forcing associated with atmospheric carbon dioxide concentration C (in parts per million by volume) is represented using the logarithmic relationship established by Myhre et al. (1998),

$$F_{\mathrm{CO_2}}(t) = F_{2\times}\,\frac{\ln\bigl(C(t)/C_0\bigr)}{\ln 2}, \tag{4}$$

where $C_0 = 280\,\mathrm{ppm}$ is the preindustrial baseline concentration and $F_{2\times} = 3.71\,\mathrm{W\,m^{-2}}$ is the forcing associated with a doubling of CO_2. This parameterization captures the saturation behavior of the CO_2 absorption bands in the infrared and has been validated against line-by-line radiative transfer calculations.

3.2 Atmospheric CO_2 Dynamics

The time evolution of atmospheric carbon dioxide concentration is governed by the mass balance

$$\frac{dC}{dt} = \alpha\,E(t) - S_{\mathrm{land}}(T_m, C, \phi) - S_{\mathrm{ocean}}(T_m, C) - L(C), \tag{5}$$

where:

- $E(t)$ $[\mathrm{Pg\,C\,yr^{-1}}]$ represents anthropogenic emissions,

- $\alpha \in (0, 1)$ is the airborne fraction of emitted carbon,
- S_{land} is the terrestrial carbon uptake function (Section 3.3),
- S_{ocean} is the oceanic uptake function (Section 3.4), and
- $L(C)$ represents long-timescale geological carbon removal (rock weathering and carbonate burial), treated here as a small linear term $L = \ell_0(C - C_0)$ with $\ell_0 \ll 1$.

The factor α converts from units of $\mathrm{PgC\,yr^{-1}}$ to $\mathrm{ppm\,yr^{-1}}$ using the stoichiometric relation $1\,\mathrm{Pg\,C} \approx 0.4706\,\mathrm{ppm}$.

3.3 Terrestrial Carbon Uptake

The terrestrial carbon sink depends on three interacting factors: the CO_2 fertilization of plant growth, temperature stress on soil carbon, and the fraction of land remaining in biologically productive form. These mechanisms are represented by the multiplicative expression

$$S_{\text{land}}(T_m, C, \phi) = \phi\, S_{\text{land}}^{(0)}\,(1 + \beta_{\text{fert}}\,(C - C_0))\exp\big(-\gamma_T\,\max(T_m, 0)\big), \tag{6}$$

where:

- $S_{\text{land}}^{(0)}$ $[\mathrm{Pg\,C\,yr^{-1}}]$ is the baseline terrestrial sink at preindustrial conditions,
- $\phi \in [0, 1]$ is the productive land fraction (Section 5),
- β_{fert} $[\mathrm{ppm^{-1}}]$ is the CO_2 fertilization gain coefficient, and
- γ_T $[\mathrm{K^{-1}}]$ is a temperature sensitivity parameter governing the suppression of soil carbon storage by warming.

The exponential temperature term in (6) is a simplified form of the Lloyd–Taylor respiration model (Lloyd and Taylor, 1994) and reflects empirical evidence that soil carbon decomposition accelerates with temperature (Davidson and Janssens, 2006; Parton et al., 1987). The CO_2 fertilization term captures enhanced gross primary production under elevated carbon dioxide, though its magnitude remains uncertain across biomes.

3.4 Oceanic Carbon Uptake

Oceanic carbon uptake is represented as a function of atmospheric carbon concentration and surface ocean warming,

$$S_{\text{ocean}}(T_m, C) = S_{\text{ocean}}^{(0)}\,(1 - \mu_T\,\max(T_m, 0))\,, \tag{7}$$

where $S_{\text{ocean}}^{(0)}$ is the baseline oceanic sink and μ_T parameterizes the suppression of ocean uptake by surface warming through reduced CO_2 solubility and stratification-induced reduction of the biological pump. Comprehensive Earth system model studies have shown that ocean carbon uptake efficiency declines with warming (Friedlingstein et al., 2014).

4 Nitrous Oxide Dynamics

Nitrous oxide (N_2O) is the third most important long-lived anthropogenic greenhouse gas, with a global warming potential approximately 273 times that of CO_2 over a 100-year horizon (IPCC AR6). Its primary anthropogenic sources are agricultural soils, livestock waste management, and industrial processes. Atmospheric removal occurs principally through photolysis and reaction with excited oxygen atoms in the stratosphere.

4.1 Atmospheric Mass Balance

The evolution of atmospheric N_2O concentration N (in parts per billion by volume) is governed by

$$\frac{dN}{dt} = E_N(t) - \frac{N(t)}{\tau_N}, \tag{8}$$

where $E_N(t)$ [ppb yr^{-1}] represents the anthropogenic source term and τ_N [yr] is the effective atmospheric lifetime governing stratospheric photochemical destruction. The current atmospheric lifetime is approximately 116 years, but recent work by Prather and Wilson (2026) demonstrates that uncertainty in stratospheric circulation and loss chemistry introduces additional variability into long-term projections of N_2O concentration.

4.2 Radiative Forcing from N_2O

Radiative forcing from nitrous oxide is represented using a linearized approximation about the preindustrial concentration N_0,

$$F_{\mathrm{N_2O}}(t) = k_N \left(N(t) - N_0\right), \tag{9}$$

where k_N [W m^{-2} ppb^{-1}] is an empirical forcing coefficient and $N_0 = 270$ ppb is the preindustrial baseline. This approximation is adequate for the concentration ranges considered here; a more accurate parameterization that accounts for overlapping absorption with methane is available but introduces additional complexity without changing the qualitative behavior of the system.

Remark 2. *Equation (8) admits the analytical steady state $N^* = E_N^{\infty} \cdot \tau_N$, where E_N^{∞} is the long-run emission rate. This reveals that N_2O accumulates proportionally to its lifetime: even modest reductions in τ_N caused by stratospheric changes could meaningfully reduce long-run concentrations without requiring emission reductions.*

5 Urban Infrastructure and Land Transformation

5.1 Infrastructure Growth Trajectories

Urban infrastructure expansion is represented through the time-dependent built fraction $\xi(t) \in [0, 1]$, defined as the proportion of total land area converted to impervious or built surfaces. The complementary productive land fraction entering equation (6) is

$$\phi(t) = 1 - \xi(t). \tag{10}$$

Rather than prescribing a specific functional form, the model treats $\xi(t)$ as a scenario-dependent trajectory. In the baseline scenario, ξ grows linearly from an initial value at low rate, reflecting moderate continued urbanization. Rapid infrastructure scenarios allow faster growth toward a higher ceiling. Restoration scenarios specify a declining ξ, representing depaving and ecological rehabilitation programs.

Global empirical studies suggest that urban land area is growing at rates that substantially exceed population growth rates in many regions, a phenomenon sometimes termed "land-inefficient urbanization" (Angel et al., 2011). Projections to 2030 indicate that urban extent could nearly triple relative to 2000 levels in some regions under high-growth scenarios (Seto et al., 2012).

5.2 Thermal Forcing from Built Surfaces

Built surfaces modify local and regional energy budgets through multiple mechanisms: reduced albedo increases absorbed solar radiation; reduced evapotranspiration decreases latent heat flux; anthropogenic heat from buildings and transport adds directly to the local energy balance; and altered roughness length modifies turbulent mixing (Oke, 1982). Collectively these processes constitute the urban heat island effect, whose intensity scales with urban area and population density (Zhao et al., 2014).

In the reduced-form model, these effects are aggregated into a single forcing term,

$$F_{\text{built}}(t) = f_{\text{UHI}}\, \xi(t), \tag{11}$$

where f_{UHI} [$\mathrm{W\,m^{-2}}$] is an effective forcing coefficient per unit built fraction. The parameter value used here is conservative relative to regional UHI estimates; the model is most naturally interpreted as capturing a global land-average effect rather than local urban temperatures.

6 Coupled System and Parameter Calibration

6.1 Governing Equations

The full model couples the climate, carbon, and nitrous oxide components through total radiative forcing,

$$F_{\text{tot}}(t) = F_{\text{CO}_2}(t) + F_{\text{N}_2\text{O}}(t) + F_{\text{built}}(t). \tag{12}$$

Substituting the forcing decomposition into the energy balance equations (1)–(2) and coupling to the atmospheric composition equations (5) and (8) yields the complete initial value problem

$$C_m \frac{dT_m}{dt} = F_{\text{tot}}(T_m, T_d, C, N, t) - \lambda\, T_m - \kappa\,(T_m - T_d), \tag{13}$$

$$C_d \frac{dT_d}{dt} = \kappa\,(T_m - T_d), \tag{14}$$

$$\frac{dC}{dt} = \alpha\, E(t) - S_{\text{land}}(T_m, C, \phi(t)) - S_{\text{ocean}}(T_m, C) - \ell_0(C - C_0), \tag{15}$$

$$\frac{dN}{dt} = E_N(t) - \frac{N}{\tau_N}, \tag{16}$$

with initial conditions $(T_m(0), T_d(0), C(0), N(0)) = (0, 0, C_0, N_0)$, representing a preindustrial reference state. The state vector $\mathbf{y} = (T_m, T_d, C, N)^\top \in \mathbb{R}^4$ evolves over a multi-century simulation horizon $t \in [0, T]$.

Feedback structure. The system exhibits two primary feedback loops. First, rising C increases F_{CO_2}, warming T_m, which suppresses S_{land} through the exponential term in (6), allowing C to rise further—a positive climate–carbon feedback. Second, rising ξ simultaneously reduces ϕ (weakening S_{land}) and increases F_{built}, amplifying T_m—a positive infrastructure–climate feedback that compounds the first.

6.2 Parameter Values

Table 1 summarizes the default parameter values used in the numerical experiments. Climate parameters are calibrated against CMIP5 model output following Geoffroy et al. (2013). Carbon cycle parameters are drawn from observational constraints on global carbon budgets (Canadell et al., 2007; Ciais et al., 2013) and empirical soil carbon studies (Parton et al., 1987; Lloyd and Taylor, 1994).

7 Scenario Experiments and Results

7.1 Scenario Definitions

The model is integrated numerically over a 200-year horizon using a fourth-order Runge–Kutta solver with relative and absolute tolerances of 10^{-8} and 10^{-10}, respectively. Four scenarios are defined by distinct combinations of emission trajectories and infrastructure growth pathways.

Scenario B (Baseline). Anthropogenic CO_2 emissions peak around mid-century and decline at a moderate rate consistent with policy-aligned mitigation. Infrastructure expansion follows a low-growth trajectory. This scenario represents a plausible continuation of current trends under existing climate commitments.

Scenario R (Rapid Infrastructure). Emissions decline more slowly than in the baseline, and infrastructure expansion proceeds more aggressively, with the built fraction $\xi(t)$ reaching substantially higher values by century end. This scenario explores the compounding effect of simultaneous carbon accumulation and land conversion.

Table 1: Default parameter values for the coupled eco-climate model.

Parameter	Symbol	Value	Source / Rationale
Mixed-layer heat capacity	C_m	$8\,\mathrm{W\,yr\,m^{-2}\,K^{-1}}$	Geoffroy et al. (2013)
Deep-ocean heat capacity	C_d	$100\,\mathrm{W\,yr\,m^{-2}\,K^{-1}}$	Geoffroy et al. (2013)
Net feedback parameter	λ	$1.13\,\mathrm{W\,m^{-2}\,K^{-1}}$	Geoffroy et al. (2013)
Inter-layer exchange	κ	$0.73\,\mathrm{W\,m^{-2}\,K^{-1}}$	Geoffroy et al. (2013)
CO_2 doubling forcing	$F_{2\times}$	$3.71\,\mathrm{W\,m^{-2}}$	Myhre et al. (1998)
Preindustrial CO_2	C_0	280 ppm	Observational record
Preindustrial N_2O	N_0	270 ppb	Observational record
N_2O lifetime	τ_N	116 yr	Prather and Wilson (2026)
N_2O forcing coeff.	k_N	$3.1 \times 10^{-3}\,\mathrm{W\,m^{-2}\,ppb^{-1}}$	Linearized IPCC AR6
Airborne fraction	α	0.45	Canadell et al. (2007)
Baseline land sink	$S^{(0)}_{\mathrm{land}}$	$2.5\,\mathrm{Pg\,C\,yr^{-1}}$	Ciais et al. (2013)
Baseline ocean sink	$S^{(0)}_{\mathrm{ocean}}$	$2.2\,\mathrm{Pg\,C\,yr^{-1}}$	Ciais et al. (2013)
CO_2 fertilization	β_{fert}	$1.5 \times 10^{-3}\,\mathrm{ppm^{-1}}$	Friedlingstein et al. (2014)
Temperature suppression	γ_T	$0.04\,\mathrm{K^{-1}}$	Davidson and Janssens (2006)
UHI forcing coefficient	f_{UHI}	$0.15\,\mathrm{W\,m^{-2}}$	Zhao et al. (2014)
Ocean warming sensitivity	μ_T	$0.01\,\mathrm{K^{-1}}$	Friedlingstein et al. (2014)

Scenario E (Ecological Restoration). Emissions decline rapidly through strong decarbonization. Infrastructure expansion slows and reversal of built surfaces begins mid-century, increasing ϕ and thereby strengthening terrestrial carbon uptake. This scenario represents an upper bound on the benefit achievable through combined emissions and land-use policy.

Scenario N (Elevated N_2O). Emissions follow the baseline trajectory, but N_2O emissions grow over time, reflecting continued agricultural intensification. This scenario isolates the contribution of trace-gas accumulation to long-run warming.

7.2 Temperature and Forcing Trajectories

Figure 1 presents the evolution of mixed-layer temperature anomaly T_m, total radiative forcing F_{tot}, atmospheric CO_2 concentration, and atmospheric N_2O concentration across all four scenarios.

Scenario E consistently produces the lowest temperature trajectory, reflecting both reduced emissions and enhanced terrestrial carbon uptake from restored productive land. Scenario R diverges most substantially from the baseline on multi-decadal timescales as the compound effect of reduced land sink and elevated built-surface forcing accumulates. The separation between Scenario N and the baseline illustrates the independent contribution of N_2O forcing even in the absence of changes to the carbon cycle.

7.3 Carbon Cycle Feedbacks and Land Transformation

Figure 2 presents the terrestrial carbon dynamics across scenarios, showing the productive land fraction $\phi(t)$, the instantaneous land sink $S_{\text{land}}(t)$, and the cumulative combined biosphere–ocean carbon uptake.

The center panel of Figure 2 illustrates that land sink strength is governed by a competition between CO_2 fertilization (which tends to increase uptake) and temperature suppression combined with land conversion (which tends to decrease it). In Scenario R, the depletion of productive land dominates, causing the terrestrial sink to decline despite rising atmospheric CO_2. In Scenario E, the restoration of ϕ combined with CO_2 fertilization produces enhanced uptake that partially offsets emissions.

The cumulative uptake panel demonstrates that these differences compound over time. By the end of the simulation, the gap between Scenario R and Scenario E represents a substantial difference in total atmospheric carbon burden, mediated entirely through land-use dynamics rather than differences in direct emissions trajectories.

7.4 Sensitivity Analysis: Climate Feedback and Phase Structure

Figure 3 presents two complementary views of the model's parametric structure. The left panel shows the phase portrait of the two-layer climate system in the (T_m, T_d) plane for the baseline scenario, with trajectory color indicating calendar year. The right panel shows the ECS as a function of the net feedback parameter λ.

The phase portrait reveals the characteristic two-timescale structure of the two-layer EBM: T_m responds rapidly to forcing changes while T_d lags substantially, converging toward T_m

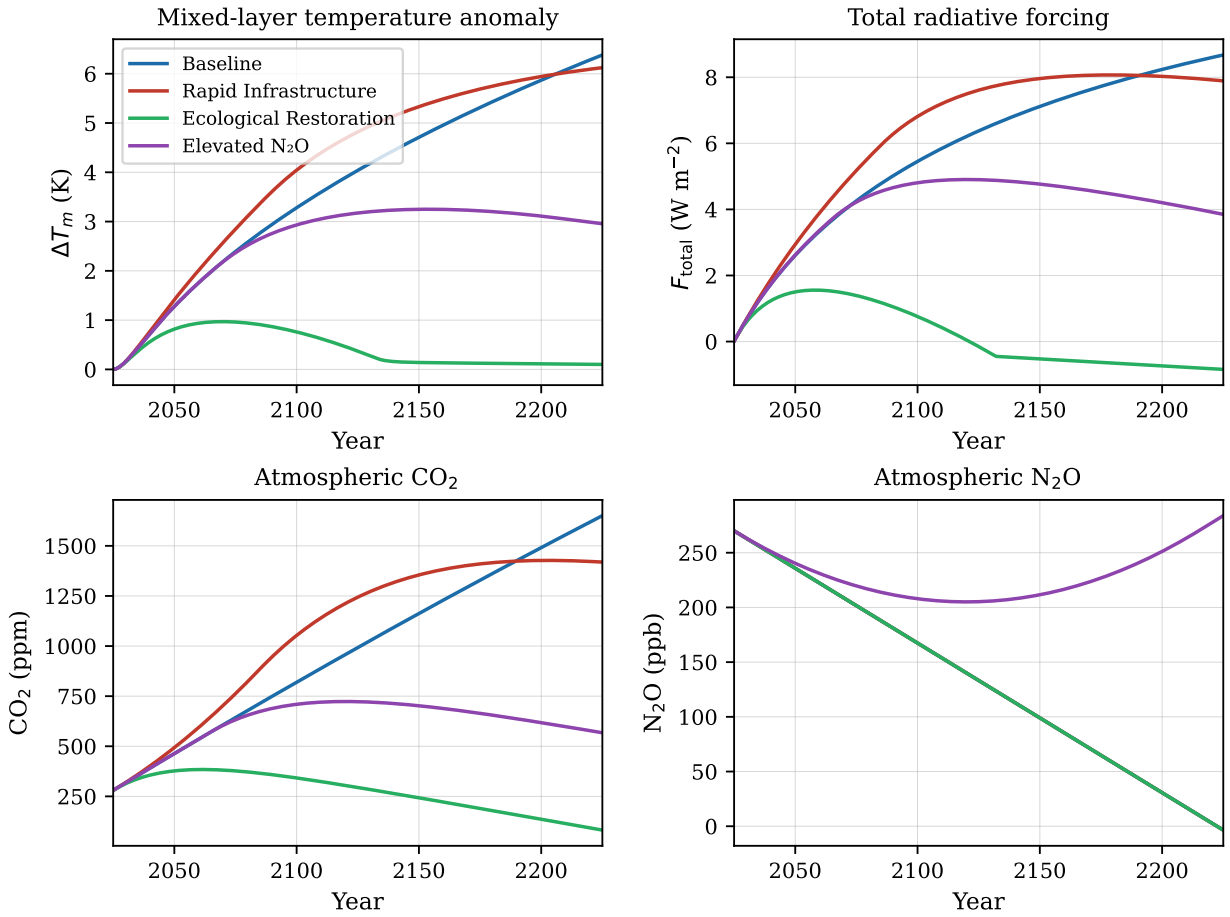

Figure 1: Two-century evolution of key model variables across four scenarios. **Top left**: Mixed-layer temperature anomaly T_m relative to a preindustrial baseline. **Top right**: Total radiative forcing F_{tot}, decomposed into CO_2, N_2O, and built-surface contributions. **Bottom left**: Atmospheric CO_2 concentration. **Bottom right**: Atmospheric N_2O concentration. The rapid infrastructure scenario (Scenario R) produces the highest long-run temperature and CO_2, while ecological restoration (Scenario E) achieves the lowest. The elevated N_2O scenario (Scenario N) tracks the baseline in CO_2 but diverges in forcing due to trace-gas accumulation.

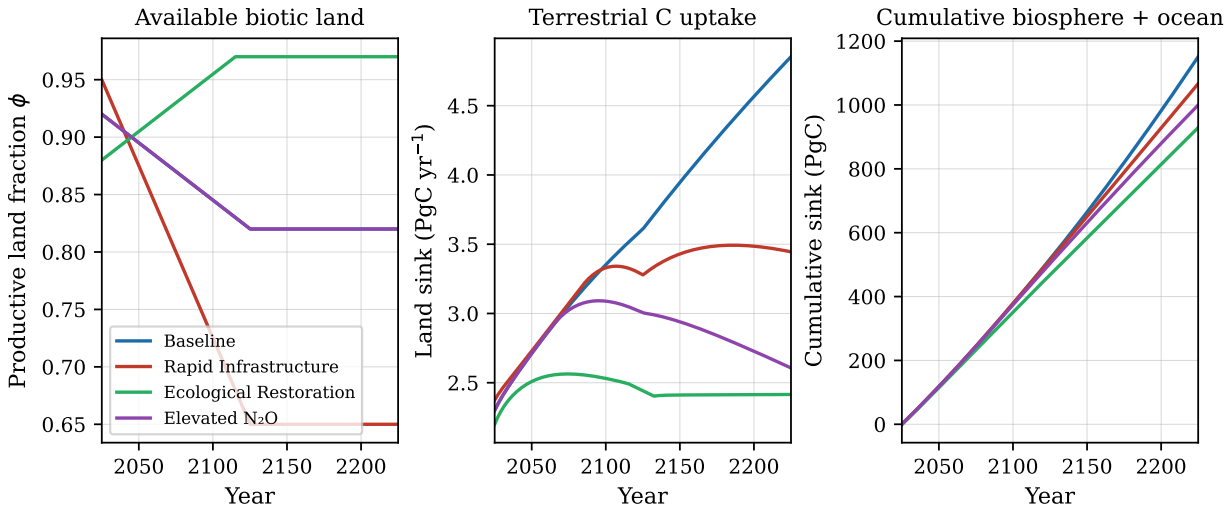

Figure 2: Carbon cycle feedbacks associated with land transformation. **Left**: Productive land fraction $\phi(t) = 1 - \xi(t)$ across scenarios. Restoration (Scenario E) recovers productive land while rapid infrastructure (Scenario R) depletes it. **Center**: Terrestrial carbon sink S_{land} (PgC yr^{-1}) as a function of time, reflecting the combined influence of ϕ, CO_2 fertilization, and temperature suppression. **Right**: Cumulative biosphere and ocean carbon uptake (PgC). The divergence between scenarios grows over time, illustrating how infrastructure-mediated land loss produces a persistent weakening of natural carbon sequestration.

only on centennial timescales. The trajectory approaches the equilibrium manifold $T_m = T_d$ asymptotically, consistent with the analytical steady-state result established in Section 2.

The ECS curve in the right panel illustrates the profound sensitivity of long-run warming to uncertainty in the feedback parameter λ. For values below approximately $0.8\,\text{W m}^{-2}\,\text{K}^{-1}$, the ECS exceeds 4 K, entering a regime of high climate sensitivity that fundamentally alters the character of long-term projections. This parametric uncertainty underscores the importance of reducing uncertainty in cloud and other feedback processes.

8 Discussion

8.1 Infrastructure as a Secondary Climate Forcing

The modeling framework developed here emphasizes a perspective that is largely absent from conventional sectoral emissions accounting: urban infrastructure constitutes not only a driver of greenhouse gas emissions but also a physical modifier of planetary energy balance and terrestrial carbon uptake capacity.

In the scenario experiments, the difference between Scenario R and Scenario B arises entirely from the rate of infrastructure expansion and its land-conversion consequences, not from differences in direct CO_2 emissions. The compound effect of reduced ϕ and elevated F_{built} produces a warming increment that accumulates over time. This suggests that infrastructure policy— decisions about urban form, building materials, road networks,

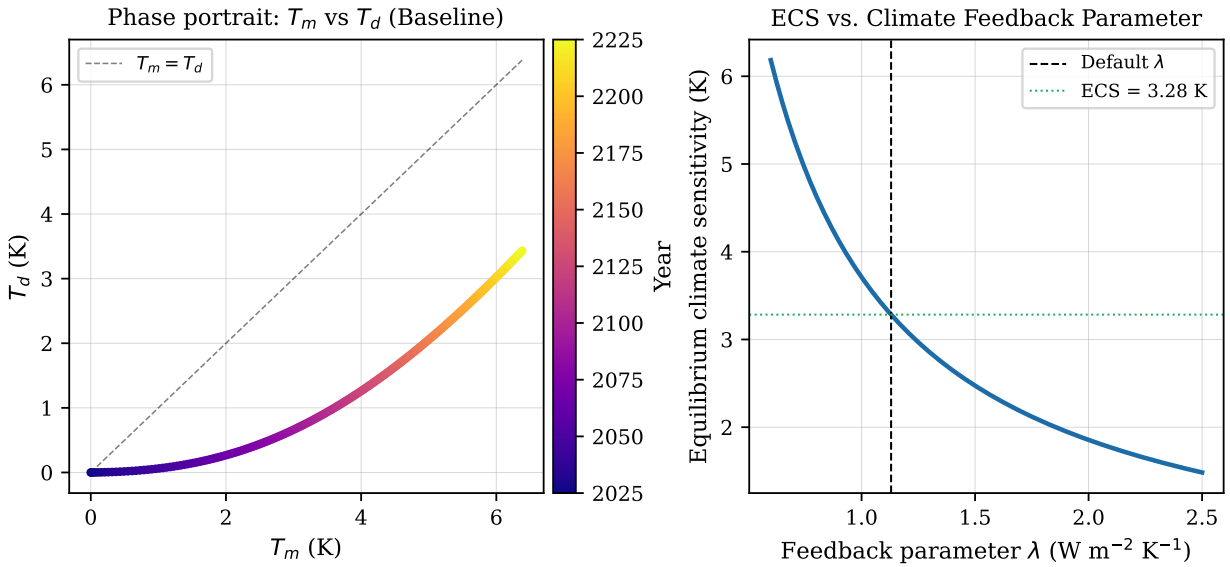

Figure 3: Structural analysis of the climate component. **Left**: Phase portrait of the two-layer energy balance model in the (T_m, T_d) plane for Scenario B, with trajectory color indicating calendar year. The diagonal dashed line marks $T_m = T_d$, the eventual equilibrium manifold. The slow convergence of T_d toward T_m illustrates deep-ocean heat uptake lag. **Right**: Equilibrium climate sensitivity (ECS, in K) as a function of the net feedback parameter λ. The dashed vertical and horizontal lines mark the default parameter value and its corresponding ECS. The steep curvature at low λ reflects the high sensitivity of the ECS to feedback uncertainty in the stabilizing regime.

and land-use planning—may have climate consequences that are currently underweighted in integrated assessment frameworks.

The mechanism operates through what might be termed a *sink suppression pathway*: as built area expands, the fraction of land available for photosynthesis and carbon storage shrinks, reducing the efficiency with which the biosphere absorbs anthropogenic emissions. Even if emissions remain identical across scenarios, weakened sink strength implies higher atmospheric carbon concentration and commensurately greater warming.

8.2 Limitations and Model Assumptions

Several simplifications limit the quantitative precision of the present framework.

Spatial homogeneity. The model treats all land as a homogeneous carbon-absorbing medium. In reality, the carbon value of land converted to built use depends strongly on the ecosystem type displaced—forests, wetlands, and peatlands store substantially more carbon than grasslands or degraded agricultural land. Spatially resolved land-use data would be necessary for quantitative projections.

Urban metabolism. The framework does not represent energy flows within urban systems—electricity generation, industrial processes, heating and cooling demands—which are the dominant pathways through which cities contribute to greenhouse gas emissions. The present model focuses instead on land-transformation feedbacks, which complement rather than substitute for conventional emission accounting.

Dynamic vegetation. The terrestrial sink representation is static in its ecological structure, lacking vegetation succession, disturbance dynamics, and nutrient limitations. More comprehensive carbon cycle models represent these processes explicitly (Parton et al., 1987), and their omission here means that long-term sink behavior may be over- or under-estimated.

Feedback sign uncertainty. The sign and magnitude of certain feedbacks—particularly CO_2 fertilization at high concentrations and soil respiration temperature sensitivity—remain empirically uncertain (Davidson and Janssens, 2006). The sensitivity analysis in Figure 3 addresses parametric uncertainty in the climate feedback parameter, but a fuller uncertainty quantification would propagate uncertainty through all parameters jointly.

8.3 Directions for Extension

The framework provides a foundation for several natural extensions. First, spatially explicit land-use data could replace stylized $\xi(t)$ trajectories, connecting the model to empirically observed urban expansion patterns (Seto et al., 2012; Angel et al., 2011). Second, the carbon cycle component could be extended to represent multiple soil and vegetation pools following CENTURY-style model architecture (Parton et al., 1987), improving the representation of soil carbon dynamics. Third, additional forcing agents—aerosols, methane, and short-lived climate pollutants associated with urban areas—could be incorporated into the forcing

decomposition (12). Fourth, uncertainty quantification via Monte Carlo sampling across the parameter space would provide probabilistic ranges for all scenario outputs.

9 Conclusion

This paper has introduced a reduced-form eco-climate modeling framework that integrates two-layer energy balance climate dynamics, simplified carbon cycle processes, nitrous oxide chemistry, and stylized urban infrastructure growth within a coupled system of ordinary differential equations. The framework treats urban expansion not merely as a driver of greenhouse gas emissions but as a physical modifier of the Earth system operating through two distinct pathways: thermal forcing associated with built-surface energy budgets, and suppression of terrestrial carbon uptake through land conversion.

Numerical experiments across four illustrative scenarios demonstrate that infrastructure dynamics can produce climatically significant divergence in temperature trajectories over multi-century time horizons even when direct emissions trajectories are held fixed. The compound effect of reduced productive land fraction and elevated built-surface forcing creates a persistent positive feedback that amplifies warming relative to a baseline in which land-use change proceeds more slowly. Conversely, scenarios that incorporate ecological restoration demonstrate that land-use policy can function as a partial substitute for emissions mitigation by enhancing the terrestrial carbon sink.

Phase portrait analysis of the two-layer energy balance model reveals the characteristic two-timescale structure underlying these dynamics: rapid surface adjustment on decadal timescales is followed by slow deep-ocean convergence on centennial timescales. Equilibrium climate sensitivity analysis demonstrates the steep dependence of long-run warming on the net climate feedback parameter, motivating continued effort to constrain cloud and other feedback processes.

The framework described here is deliberately simplified, trading quantitative precision for structural transparency. Its primary contribution is conceptual: to demonstrate that a consistent, analytically tractable system of equations can couple climate physics, ecological processes, and urban dynamics, creating a laboratory in which the interactions among these systems can be explored and understood. As global urbanization continues at rates that significantly exceed the growth of ecological restoration efforts, developing a more integrated theoretical account of how infrastructure expansion interacts with the Earth system climate will become increasingly important for long-range environmental analysis.

References

Angel, S., Parent, J., Civco, D. L., Blei, A., and Potere, D. (2011). The dimensions of global urban expansion: Estimates and projections for all countries, 2000–2050. *Progress in Planning*, 75(2):53–107.

Batty, M. (2013). *The New Science of Cities*. MIT Press, Cambridge, MA.

Canadell, J. G., Le Quéré, C., Raupach, M. R., Field, C. B., Buitenhuis, E. T., Ciais, P., Conway, T. J., Gillett, N. P., Houghton, R. A., and Marland, G. (2007). Contributions to accelerating atmospheric CO_2 growth from economic activity, carbon intensity, and efficiency of natural sinks. *Proceedings of the National Academy of Sciences*, 104(47):18866–18870.

Ciais, P., Sabine, C., Bala, G., Bopp, L., Brovkin, V., Canadell, J., Chhabra, A., et al. (2013). Carbon and other biogeochemical cycles. In *Climate Change 2013: The Physical Science Basis. Contribution of Working Group I to the Fifth Assessment Report of the IPCC*. Cambridge University Press, Cambridge, UK.

Davidson, E. A. and Janssens, I. A. (2006). Temperature sensitivity of soil carbon decomposition and feedbacks to climate change. *Nature*, 440:165–173.

Friedlingstein, P., Meinshausen, M., Arora, V. K., Jones, C. D., Anav, A., Liddicoat, S. K., and Knutti, R. (2014). Uncertainties in CMIP5 climate projections due to carbon cycle feedbacks. *Journal of Climate*, 27(2):511–526.

Geoffroy, O., Saint-Martin, D., Bellon, G., Voldoire, A., Olivié, D., and Tytéca, S. (2013). Transient climate response in a two-layer energy-balance model. Part I: Analytical solution and parameter calibration using CMIP5 AOGCM experiments. *Journal of Climate*, 26(6):1841–1857.

Gregory, J. M., Ingram, W. J., Palmer, M. A., Jones, G. S., Stott, P. A., Thorpe, R. B., Lowe, J. A., Johns, T. C., and Williams, K. D. (2004). A new method for diagnosing radiative forcing and climate sensitivity. *Geophysical Research Letters*, 31(3).

Hansen, J., Lacis, A., Rind, D., Russell, G., Stone, P., Fung, I., Ruedy, R., and Lerner, J. (1984). Climate sensitivity: Analysis of feedback mechanisms. *Geophysical Monograph Series*, 29:130–163.

Imhoff, M. L., Zhang, P., Wolfe, R. E., and Bounoua, L. (2010). Remote sensing of the urban heat island effect across biomes in the continental USA. *Remote Sensing of Environment*, 114(3):504–513.

Lloyd, J. and Taylor, J. A. (1994). On the temperature dependence of soil respiration. *Functional Ecology*, 8(3):315–323.

Myhre, G., Highwood, E. J., Shine, K. P., and Stordal, F. (1998). New estimates of radiative forcing due to well mixed greenhouse gases. *Geophysical Research Letters*, 25(14):2715–2718.

Oke, T. R. (1982). The energetic basis of the urban heat island. *Quarterly Journal of the Royal Meteorological Society*, 108(455):1–24.

Parton, W. J., Schimel, D. S., Cole, C. V., and Ojima, D. S. (1987). Analysis of factors controlling soil organic matter levels in Great Plains grasslands. *Soil Science Society of America Journal*, 51(5):1173–1179.

Prather, M. J. and Wilson, C. P. (2026). Projecting nitrous oxide over the 21st century: Uncertainty related to stratospheric loss. *Proceedings of the National Academy of Sciences*, 123(6):e2524123123.

Seto, K. C., Güneralp, B., and Hutyra, L. R. (2012). Global forecasts of urban expansion to 2030 and direct impacts on biodiversity and carbon pools. *Proceedings of the National Academy of Sciences*, 109(40):16083–16088.

Zhao, L., Lee, X., Smith, R. B., and Oleson, K. (2014). Strong contributions of local background climate to urban heat islands. *Nature*, 511:216–219.